

DOI: 10.1002/celec.201300013

Directly Grown $K_{0.33}WO_3$ Nanosheet Film Electrode for Fast Direct Electron Transfer of Protein

Jinping Liu,^[b] Lei Liao,^[c] Zhisong Lu,^[a] Bin Yan,^[d] Ting Yu,^[d] Zhe Zheng,^[d] Jixuan Zhang,^[e] Hao Gong,^[e] Xintang Huang,^[b] and Chang Ming Li^{*[a]}

A potassium tungstate ($K_{0.33}WO_3$) nanosheet film grown directly on a conductive tungsten (W) substrate by a hotplate-heating approach effects direct electron transfer between the W electrode and a biocatalytic protein or microbe, a long-sought effect of both fundamental and practical importance. The $K_{0.33}WO_3$ forms into a 5–20 nm thick multilayered nanosheet with a number of steps along the surface. A single nanosheet of $K_{0.33}WO_3$ is hydrophilic and highly electron conducting (resistivity $\sim 8.3 \times 10^{-3} \Omega \text{ cm}$), characteristic of metallic behaviour. Glucose oxidase (GOD) immobilized on a $K_{0.33}WO_3$ -nanosheet-

coated electrode demonstrates facile direct electron transfer. The electron transfer rate constant (k_s) is $\sim 9.5 \text{ s}^{-1}$. This electrode has been used to construct a direct electrochemistry-based glucose sensor, which exhibits good sensitivity (as high as $\sim 66.4 \mu\text{A mm}^{-2} \text{ cm}^{-2}$), fast sensing response time ($\sim 4 \text{ s}$), a low detection limit ($0.5 \mu\text{M}$), high selectivity and good reliability in practical uses. Growing $K_{0.33}WO_3$ nanosheet on electrodes offers a promising general approach for effecting direct bioelectrochemistry for widespread uses in bioelectronic and bioenergy applications.

1. Introduction

Direct electrochemistry, the direct electron transfer between electrode and protein or microbe has been extensively studied due to not only its fundamental importance in biological organisms and bioelectrochemistry, but also due its remarkable potential applications in biofuel cells,^[1,2] biosensors^[3–8] and bioelectronics.^[11] Nevertheless, it often encounters a major obstacle resulting from the deeply embedded redox centers in a surrounding “insulation layer” of a protein or microbe.^[1,9] Thereby, it is of great importance to shorten the electron-tunneling dis-

tance between the redox center of the protein/microbe and the electrode to enable direct electron transfer.^[9] Recent studies have demonstrated that direct electrochemistry can be realized by uniquely nanostructured electrodes,^[10–24] which could access the embedded redox centers of proteins or microbes while increasing surface area, enhancing mass transport and controlling the electrode microenvironment.^[1,10–14] Further, some physico-chemical properties, including conductivity, hydrophilicity and interfacial resistance are essential to enhance the direct electron transfer rate.^[18,25–27] Conductive nanostructures such as various carbon nanomaterials^[10–14] and noble metal (Au/Pt) nanoparticles^[15–17] have been utilized on the electrode surface to facilitate the direct electron transfer of proteins, but they are expensive and hydrophobic. Hydrophobicity is often a serious problem that makes it difficult for the reactant in an aqueous solution to access the reaction sites on the electrode surface.^[11] Highly porous metal oxide nanostructures (TiO_2 , ZnO , etc.)^[8,18–20] and some layered inorganic materials (clay, phosphates, titanate)^[21–24] are superior to many carbon and metal nanostructures in hydrophilicity and sometimes in specific surface area. However, a lack of good electrical conductivity limits their performance in direct electrochemistry. The conductivity and hydrophilicity may be improved by incorporation of hydrophilic or/and conductive materials into electrodes^[12–17] or functionalization of electrode surfaces.^[1,10,11] These approaches often involve a complicated process and could result in low stability and poor reproducibility. In addition, the significant interfacial resistance introduced by coating or depositing nanostructure material onto an electrode surface could also greatly inhibit direct electrochemistry.^[6,26] There is a great challenge to economically fabricate an advanced material with novel nanostructure, good conductivity, high hydro-

[a] Dr. Z. S. Lu, Prof. C. M. Li
Chongqing Key Laboratory for Advanced Materials &
Technologies of Clean Energies
Institute for Clean Energy & Advanced Materials
Southwest University
Chongqing 400715 (P. R. China)
E-mail: ecml@swu.edu.cn


[b] Dr. J. P. Liu,[†] Prof. X. T. Huang
Institute of Nanoscience and Nanotechnology
Department of Physics, Central China Normal University
Wuhan 430079 (P. R. China)

[c] Prof. L. Liao[†]
School of Physics and Technology, Wuhan University
Wuhan 430072 (P. R. China)

[d] Dr. B. Yan, Dr. T. Yu, Dr. Z. Zheng
Division of Physics and Applied Physics
School of Physical and Mathematical Sciences
Nanyang Technological University
Singapore 637371 (Singapore)

[e] Dr. J. X. Zhang, Dr. H. Gong
Department of Materials Science and Engineering
National University of Singapore
Singapore 117576 (Singapore)

[†] These authors contributed equally to this work.

 Supporting information for this article is available on the WWW under <http://dx.doi.org/10.1002/celec.201300013>.

philicity, large specific surface area and low interfacial resistance.^[28–30] As a promising solution to the challenge, in this work, direct growth of a unique conductive and hydrophilic nanostructured material on an electrode surface is conducted to eliminate the tedious process conventionally used in electrode fabrication with use of polymer binders, while providing stronger adhesion and better electrical contact to significantly reduce the interfacial resistance caused by the nonconductive binder and loose electrical contact. This also offers an opportunity to fabricate completely integrated bioelectronic systems. A possible mechanism to explain the fast direct electron transfer between the unique nanostructured material and protein is proposed.

Tungsten bronzes, non-stoichiometric compounds with a general formula $A_x\text{WO}_3$ ($0 < x < 1/3$),^[31] where A can be an alkali metal, lead, thallium, copper, silver, or a lanthanide, have shown interesting photochromic, electro-optic and superconducting properties.^[31–33] In particular, hexagonal potassium tungsten bronzes $K_x\text{WO}_3$ have attracted growing attention with respect to nanostructures and physical properties (such as polarized micro-Raman scattering and electron field emission) in the past few decades.^[34–40] However, their potential applications, especially their biosensing applications have never been exploited. Nanosheets, which are ultrathin, a high surface-to-volume ratio and interesting functions, are one type of ideal nanostructure to fabricate nanodevices.^[41–43]

Herein we demonstrate the direct growth of a novel $K_{0.33}\text{WO}_3$ nanosheet from tungsten (W) foil. Interestingly, owing to its unique structure, the $K_{0.33}\text{WO}_3$ nanosheet exhibits excellent electrical conductivity, good hydrophilicity and biocompatibility, making it an ideal candidate to immobilize proteins for direct electron transfer. Biosensors have continued to fuel great interest in recent years for their important applications in clinical diagnosis, environmental monitoring and food quality control.^[44–47] Direct-electrochemistry-based enzymatic biosensors^[3–8] can offer high sensitivity due to their fast electron transfer rates and superior selectivity, as the low redox potential reduce or eliminate interference reactions.^[9] As a model example, we demonstrate herein an as-grown $K_{0.33}\text{WO}_3$ nanosheet film electrode that simultaneously possesses good conductivity, high hydrophilicity and low interfacial resistance for fast direct electrochemistry of glucose oxidase (GOD), thus leading to a novel direct-electrochemistry-based glucose biosensor with very high sensitivity and low detection limit in the presence of interfering agents, among the best ones to date in both cost and sensing performance.

2. Results and Discussion

2.1. Structure, Electronic Conductivity and Hydrophilicity

The morphology of the as-prepared sample was examined by using field-emission scanning electron microscopy (FE-SEM). After heating at 600 °C for 24 hours in air, the pre-treated W foil was uniformly covered by ultrathin nanosheets with a thickness of 5–20 nm (Figure 1a). Figure 1b shows the X-ray diffraction (XRD) pattern of the as-grown sample. All the peaks

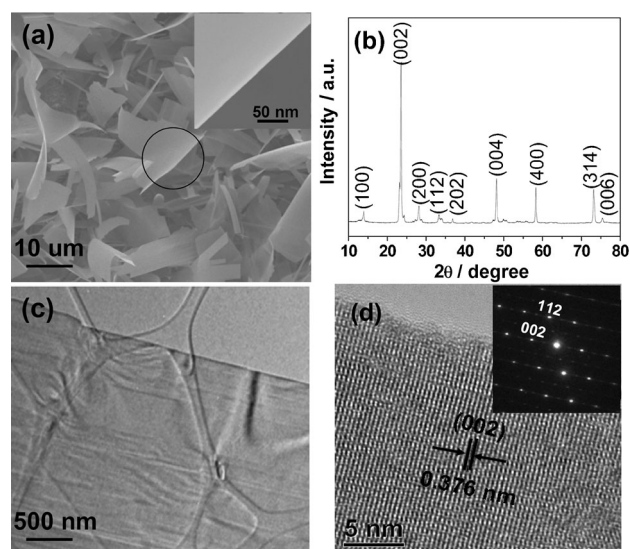


Figure 1. a) SEM image and b) XRD pattern of the as-prepared nanosheet film. The inset in (a) shows an individual sheet. c) Typical TEM image of the nanosheet. d) HRTEM image and the SAED pattern of a single nanosheet, revealing that the 2D surface is (200).

can be indexed to the pure hexagonal potassium tungsten bronze $K_{0.33}\text{WO}_3$ (JCPDS file No. 26-1345) and no impurities were identified. Figure 1c shows the typical transmission electron microscope (TEM) image of $K_{0.33}\text{WO}_3$ nanosheet, which is ultrathin and homogeneous. In the high-resolution TEM (HRTEM) image (Figure 1d), the interplanar spacing of 3.76 Å is revealed, corresponding to that of the (002) plane. The selected-area electron diffraction (SAED) pattern (inset of Figure 1d) confirms the single-crystal nature of nanosheet. From the SAED, the wide surface of nanosheet can be determined as the (200) plane.

The composition of nanosheets is further confirmed by X-ray energy-dispersive spectroscopy (EDS) analysis (Figure 2). Figures 2b–d show the elemental mapping results of the single nanosheet in Figure 2a. The images correspond to the O K-edge, W M-edge, and K K-edge signals, respectively. It can be clearly seen that potassium ions are uniformly distributed in the nanosheet at a low density. The EDS datum (Figure 2e) also indicates the presence of K, W and O elements, in which the C and Cu peaks come from the underlying carbon-coated Cu mesh.

The nanosheet thickness was further determined by atomic force microscopy (AFM). The representative AFM height image is shown in Figure 3a (inset). The height profile across the nanosheet indicates a thickness of ~15 nm, consistent with the SEM observation. Interestingly, there is a clear step on the nanosheet, with a homogeneous height of ~4 nm. It is well-known that the $K_{0.33}\text{WO}_3$ structure comprises a rigid tungsten-oxygen framework built up of units containing corner-sharing WO_6 octahedra that are arranged in six-membered rings.^[34,35] The units are stacked along the [001] axis, giving rise to one-dimensional hexagonal channels, which are occupied randomly by potassium ions (Figure 3b). Therefore, the presence of uniform step on wide surface of the sheet may be due to facet

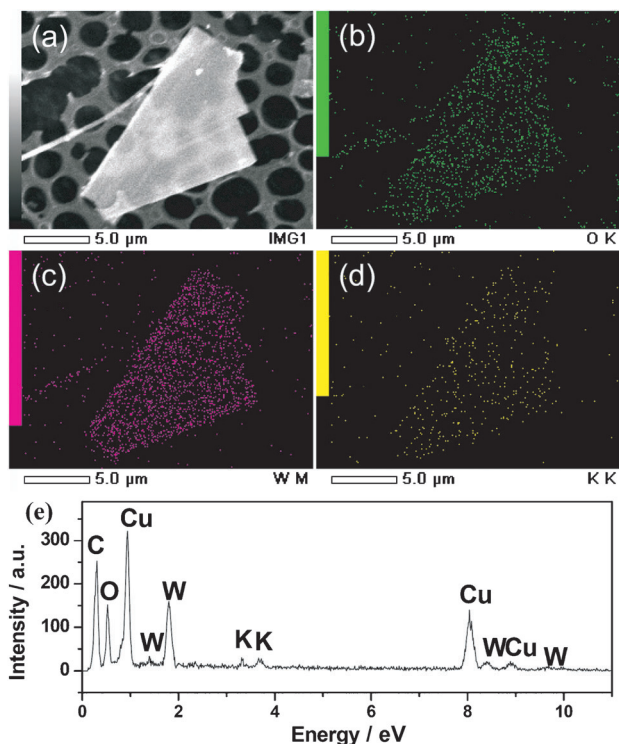


Figure 2. a) A single nanosheet. b)–d) EDS maps depict the distribution of the constituting elements within the nanosheet. e) EDS datum indicating the presence of K, W and O.

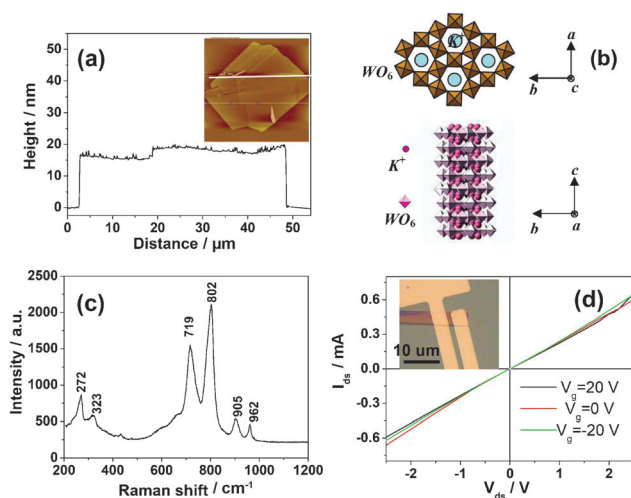


Figure 3. a) AFM height profile across a single nanosheet. Inset is the AFM height image. b) Crystal structure of $K_{0.33}WO_3$ projected along the c - and a -axes, respectively. Potassium ions occupy the hexagonal channels along c axis randomly. c) Raman spectrum of the nanosheet. d) I_{ds} versus V_{ds} curves obtained from the FET device (inset) made of a single $K_{0.33}WO_3$ nanosheet with various V_g : from -20 to 20 V.

cleavage of both (200) and (002) planes and it is a direct indication of the multilayered configuration of nanosheets. More than ten nanosheets were examined by AFM and in most cases cleavage cracks could be detected. Figure S1 (Supporting Information) shows another example where one can observe

three obvious sharp steps with an average height of ~ 3 nm on the nanosheet surface. The presence of these steps is believed to facilitate the adsorption of oxidases such as GOD.

The Raman spectrum in Figure 3c shows three groups of peaks in the regions of 900 – 1000 , 600 – 850 and 200 – 400 cm^{-1} , which can be assigned to $W=O$ stretching, $O-W-O$ stretching and $O-W-O$ bending modes, respectively.^[37] Figure 3d shows I_{ds} versus V_{ds} curves obtained from the field-effect transistor (FET) device made of a single $K_{0.33}WO_3$ nanosheet with various V_g varying from -20 to 20 V. The linear I_{ds} – V_{ds} curves indicate that the Au electrodes form good ohmic contacts with the $K_{0.33}WO_3$ nanosheet. The resistivity is about $8.3 \times 10^{-3} \Omega cm$. Compared with traditional metal oxide nanostructures (e.g. ZnO, SnO_2),^[48] the resistivity of the $K_{0.33}WO_3$ nanosheet is significantly lower (five orders of magnitude difference). Moreover, no gate effect could be observed. The high conductivity may be explained considering the crystal structure of $K_{0.33}WO_3$.^[35] As discussed above, K^+ occupies hexagonal channels formed by the stacking of many units. In $K_{0.33}WO_3$, the K^+ content is low, only the larger hexagonal channels contain K^+ . Thus K^+ can easily dwell in these channels without the distortion of the parent WO_3 framework, and provide electrons to the WO_3 lattice.^[49] This should lead to a significant decrease of resistivity and the metallic behavior.

Another remarkable property of $K_{0.33}WO_3$ nanosheet is its good hydrophilicity, as confirmed by dynamic contact angle (CA) measurements (Figure 4). When water is dropped on the

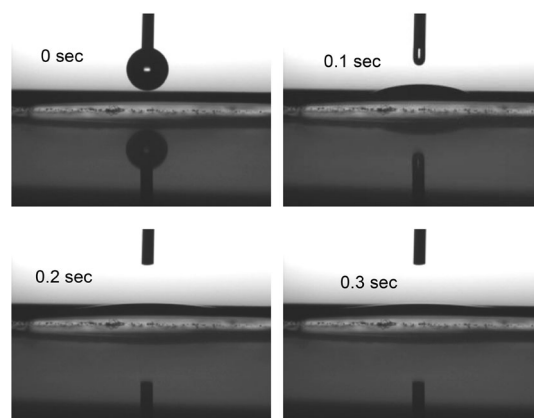


Figure 4. Change in the contact angle (CA) change of a water drop on the $K_{0.33}WO_3$ film surface.

nanosheet film surface, after only 0.3 s the CA decreases to less than 5° . A similar phenomenon can be observed when the water drop is replaced by a drop of protein solution containing GOD (15 $mg mL^{-1}$ in 0.01 M PBS, pH 7.0). It is well-known that protein molecules consist of hydrophilic and hydrophobic groups. Under biological conditions, the hydrophilic groups of the protein, such as amido and carboxyl, are exposed to the environment and the hydrophobic groups are assembled in the inner core. Thus, they can easily adsorb to the hydrophilic surfaces. The small observed CA indicates that this surface is ideal for GOD immobilization, and can provide a favorable mi-

croenvironment for the maintenance of its bioactivity. The biocompatibility was also estimated by UV/Vis absorption spectroscopy. The result revealed that there is no absorption band shift due to structural denaturation of proteins such as GOD and hemoglobin (Hb) after immobilization on the $K_{0.33}WO_3$ (Figure S2). These appealing features combined with the high electrical conductivity make $K_{0.33}WO_3$ highly suitable as a novel electrode material for direct electrochemistry of proteins and bio-applications.

2.2. Fast Direct Electron Transfer

Glucose sensors is always one of most interesting and important research areas, due to its importance in the treatment of diabetes mellitus, a group of metabolic diseases afflicting about 200 million people worldwide.^[50–53] GOD is the key sensing component for glucose detection. The direct electrochemistry of GOD involves two-electron transfer coupled with two protons.^[25] Cyclic voltammograms (CVs) of Nafion/GOD, Nafion/ $K_{0.33}WO_3$ and Nafion/GOD/ $K_{0.33}WO_3$ electrodes in N_2 -saturated phosphate buffer solution (PBS) (pH 7.0) at 0.1 V s^{-1} were investigated (Figure 5 a). Neither Nafion/GOD nor Nafion/

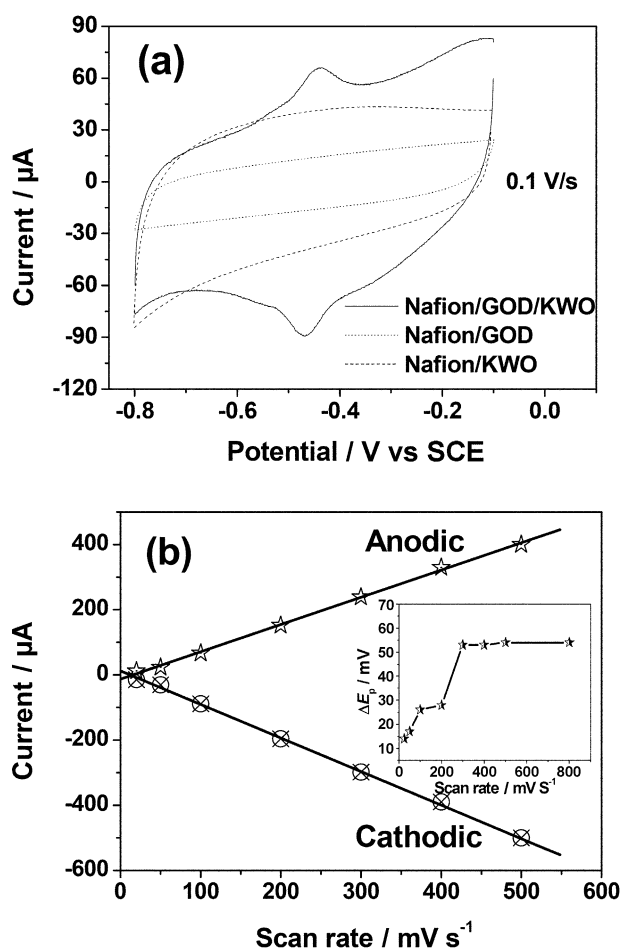


Figure 5. a) CVs of different electrodes in 0.1 M pH 7.0 N_2 -saturated PBS solutions at 0.1 V s^{-1} : Nafion/KWO; Nafion/GOD; Nafion/GOD/KWO. b) Plots of cathodic and anodic peak currents and ΔE_p versus scan rate.

$K_{0.33}WO_3$ -modified electrodes showed any redox peak. In contrast, the Nafion/GOD/ $K_{0.33}WO_3$ electrode exhibits a pair of symmetric, reversible peaks located at -0.468 and -0.441 V . This clearly indicates that direct electron transfer of GOD can be successfully achieved by the growth of $K_{0.33}WO_3$ on the W electrode surface. From the integration of the cathodic peak of the Nafion/GOD/ $K_{0.33}WO_3$ electrode at 0.1 V s^{-1} , the surface coverage of GOD calculated from $\Gamma = Q/nFA$, where Q is the charge involved in the reaction, n is the number of electron transferred, F is Faraday constant and A is the electrode area, is $2.9 \times 10^{-10}\text{ mol cm}^{-2}$. Upon increasing the scan rate from 0.02 to 0.5 V s^{-1} , the redox peak currents increase linearly at the Nafion/GOD/ $K_{0.33}WO_3$ electrode, as shown in Figure 5 b. This is a typical surface-controlled electrochemical reaction.^[25] The potential difference between the anodic and cathodic peaks (ΔE_p) increases with increasing scan rate. At scan rates of 0.05 , 0.1 and 0.2 V s^{-1} , ΔE_p is 17 , 26 and 28 mV , respectively (inset of Figure 5 b). The electron transfer rate constant (k_s) between GOD and the electrode estimated from the Laviron model^[18–20] is 9.5 s^{-1} ,^[18–20] which is much higher than those of GOD immobilized on CNTs,^[13,14,53] Au,^[15] and most inorganic nanostructure films such as highly porous TiO_2 .^[18] The above results may indicate that the $K_{0.33}WO_3$ nanosheet film does not only play an important role in stabilizing GOD by providing a friendly microenvironment, but also provides a unique nanostructure, good conductivity and high hydrophilicity to enable fast direct electron transfer.

2.3. Glucose Sensing

For the Nafion/GOD/ $K_{0.33}WO_3$ electrode, when the CV is measured in air-saturated PBS, a pair of redox peaks is still observed (Figure 6). However, the cathodic peak current increases and the anodic current decreases as compared to the result in N_2 -saturated PBS. This confirms that oxygen dissolved in the solution can be catalytically reduced by GOD-FADH₂ at the electrode.^[14] Upon addition of 1.5 mM glucose to air-saturated

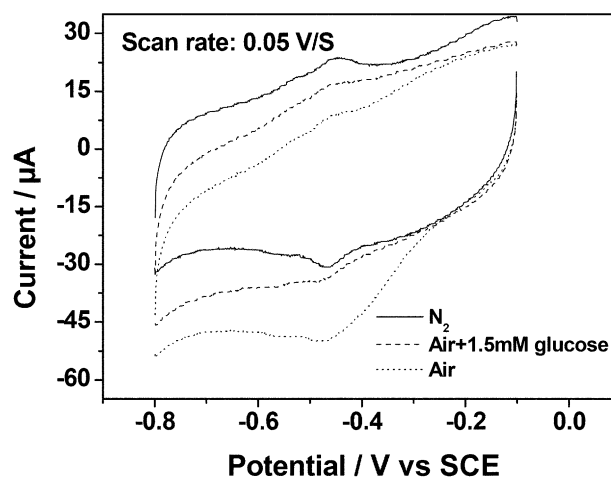


Figure 6. CVs of the Nafion/GOD/KWO electrode in N_2 - and air-saturated 0.1 M PBS solutions with and without the addition of 1.5 mM glucose. Scan rate: 0.05 V s^{-1} .

PBS, the cathodic peak current decreases as a consequence of the enzymatic reaction between GOD-FAD and glucose.^[13,14,25] There is an argument whether a glucose sensor really involves the direct electron transfer of GOD if it relies on detection of decreased amperometric responses of oxygen reduction like a Clark glucose sensor rather than directly sensing glucose oxidation through direct electron transfer between glucose oxidase and electrode.^[54,55,56] However, our work^[57] has clearly demonstrated that this type of biosensor is indeed based on the direct transfer of GOD to have high sensitivity. We now propose a detailed mechanism.

An amperometric experiment was carried out to test the biosensor performance. A typical current–time plot of the biosensor on the successive additions of glucose is illustrated in Figure 7a (potential: -0.45 V). The stepped increase of glucose concentration in buffers causes the corresponding decrease in the current, and a well-defined response is observed. Even at a low glucose concentration of $5 \mu\text{M}$, there is still an obvious decrease in the current. The average time to achieve a 95% steady-state current is ~ 4 s, indicating a fast sensing response time. The calibration plot (Figure 7b) is linear over the concen-

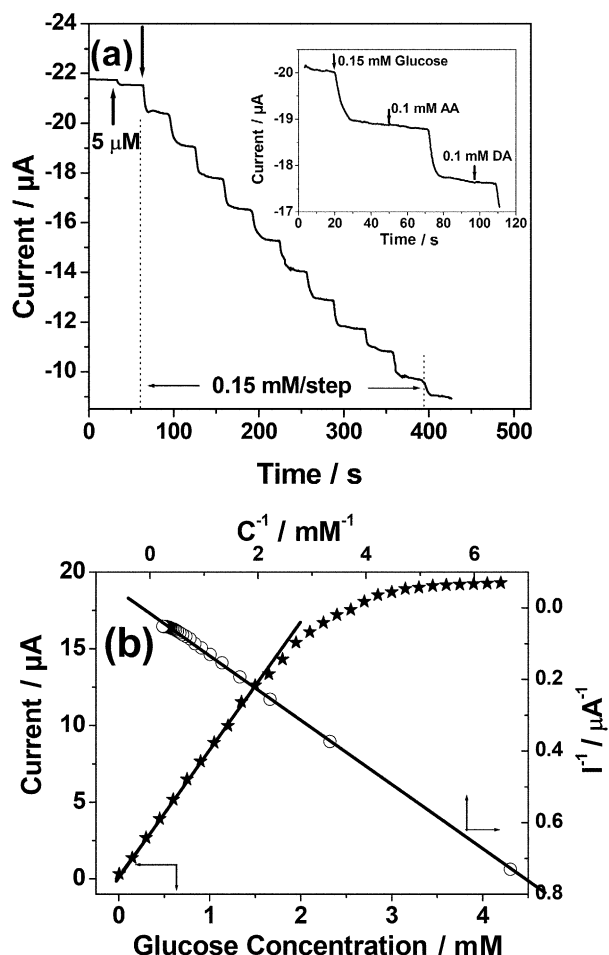


Figure 7. a) Current–time curve of the Nafion/GOD/KWO electrode for successive additions of glucose to air-saturated and stirred 0.1 M pH 7.0 PBS solution at -0.45 V. The inset shows the effect of interfering species on the biosensor response. b) Calibration curve (current versus glucose concentration) and Lineweaver–Burk plot (I^{-1} versus C^{-1}).

tration range from $5 \mu\text{M}$ to 1.5 mM , with a slope of $8.3 \mu\text{A mM}^{-1}$ and a correlation coefficient of 0.9998. The detection limit is as low as $0.5 \mu\text{M}$ at a signal-to-noise (S/N) ratio of 3. An extremely attractive feature of the $\text{K}_{0.33}\text{WO}_3$ -based biosensor is its high sensitivity, namely $66.4 \mu\text{A mM}^{-1} \text{ cm}^{-2}$. This value is superior to that reported for a glucose biosensor using a Pd/Pt-exfoliated graphite electrode,^[51] twice of that of a biosensor constructed with Pt/CNTs,^[52] and much better than those of other glucose biosensors reported in literature.^[14,18,25] When the concentration of glucose is higher, a platform emerges in the catalytic peak current, which accords with the Michaelis–Menten model. The calculated apparent Michaelis–Menten constant (K_m^{app}) is 2.05 mM based on Lineweaver–Burk equation: $1/I_m = 1/I_{\text{max}} + K_m^{\text{app}}/(cI_{\text{max}})$ (Figure 7b), where I_m is the steady-state current, I_{max} is the maximum current, and c is the glucose concentration. The small value suggests a high affinity of GOD/ $\text{K}_{0.33}\text{WO}_3$ film to glucose.^[8,20] Due to its high sensitivity and low limit of detection, this sensor can easily be tailored with various dynamic ranges for different applications.^[6,8]

The good performance of our biosensor is mainly attributable to the hydrophilicity and electrical conductivity of $\text{K}_{0.33}\text{WO}_3$ nanosheets. Hydrophilicity not only facilitates the effective immobilization and bioactivity retention of GOD on the electrode surface, but also shortens the distance for glucose to easily reach the GOD-active sites.^[11] The high electron mobility of the nanosheets and their robust electrical contact with the substrate with extremely low interfacial resistance results in rapid and easy electron transfer from biomolecules to electrode. In particular, electron transfer through these highly crystalline oriented nanosheets is expected to be faster than the percolation through the conventionally used particles. Actually, the conductive film provides an electronic circuit as a series of “conductive bridges”^[10] that accesses the redox center of GOD and connects the electrode at the same time, making it possible to reduce the electron-tunneling distance. In addition, the three-dimensional network of cleavage crack-abundant nanosheets significantly increases the surface area for more GOD immobilization, thus benefiting the sensitivity of the biosensor. On the other hand, the direct growth of $\text{K}_{0.33}\text{WO}_3$ nanosheets from the W electrode substrate ensures a good adhesion between nanosheets and substrate, which helps to maintain the operational stability of the electrode. As confirmed, there is nearly no obvious decrease of the voltammetric response after continuously scanning for 50 cycles. The excellent operational stability of electrode contributes additionally to the high performance of the biosensor. Our work opens up the possibility to develop advanced multicharacteristic electrode materials for biosensing applications.

The operation of the biosensor at -0.45 V vs SCE ensures good selectivity for glucose, which is particularly important in an implantable glucose sensor.^[4] We observed that there was no significant change of the amperometric response when 0.1 mM dopamine (DA) and ascorbic acid (AA) that commonly exist in human blood were added to the PBS solution (inset of Figure 7a). We further investigated the relationship between the sensitivity of biosensor and the GOD concentration used for immobilization. As shown in Figure 8, there is an optimal

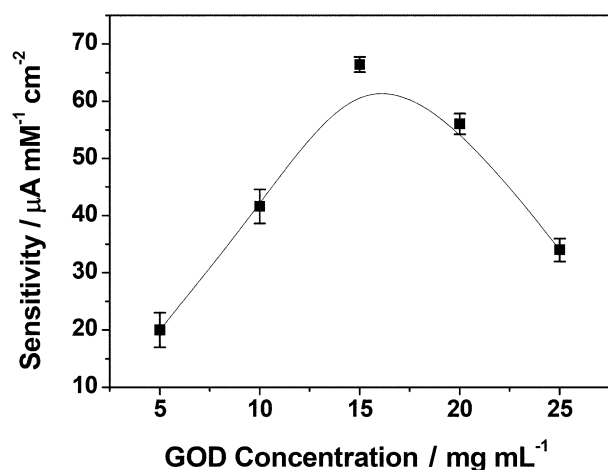


Figure 8. Biosensor sensitivity versus the GOD concentration used for immobilization.

GOD concentration (15 mg mL⁻¹). In the concentration range from 0–15 mg mL⁻¹, the higher the GOD concentration, the higher the sensitivity. Under these conditions, it is believed that the rough surface of K_{0.33}WO₃ nanosheets with numerous structural cracks are in direct contact with adsorbed GOD. However, a further increase in the GOD concentration results in the decrease of sensitivity. This is because a very high GOD loading could produce layer of GOD too thick to allow full contact with the K_{0.33}WO₃ nanostructure electrode surface, thus inhibiting direct electrochemistry. Also, with too high GOD concentrations, the operational stability was found to decrease continuously during electrochemical measurements. Obviously, the adsorption of GOD is of great importance to the performance of glucose biosensors. The adsorption profile of GOD on the nanosheets and its relationship to the sample surface area need to be further studied for better performance. In order to achieve both larger loading capacity and higher sensitivity, development of 3D structured nanosheets may be a possible strategy. The storage stability of the biosensor was studied by storing the sensor dry at 4 °C and studying the direct electrochemistry of GOD and the response to glucose. When it was stored for one week, no obvious decrease in the current for the direct electrochemistry and the response to glucose were detected. After one month, the sensor still retained 92% of its initial current response to glucose. The fabrication reproducibility of five electrodes, made independently, showed reproducibility with a relative standard deviation (RSD) of 3.5%.

The sensor was further examined in three serum samples and compared to the measured results in clinical labs. Before the analysis all the serum samples were 5-fold diluted to make the concentrations of glucose within the linear response range. The results are shown in Table 1. The two methods are in an acceptable agreement. The recoveries were also determined with the standard addition method in serum samples. In experiments, glucose standard solutions of 0.35 mM were added and mixed with the 5-fold diluted human serum samples. The recovery results further indicate good reliability of this biosensor.

Table 1. Determination of glucose concentration in serum samples.

Sample	Hospital/5-fold diluted [mM]	Present method [mM]	RSD [%], n=5	Added [mM]	Found [mM]	Recovery [%], n=5
1	0.84	0.82	-2.4	0.35	1.14	96
2	0.65	0.63	-3.1	0.35	1.02	102
3	0.98	1.02	4.1	0.35	1.29	97

Electrical conductivity and hydrophilicity are constantly demanded for electrode materials for various electrochemical devices. Although not discussed here, we believe that the K_{0.33}WO₃ nanosheet film electrode investigated in this work holds great promise in other electrochemical applications such as biofuel cells and Li-ion batteries.

3. Conclusions

In summary, a K_{0.33}WO₃ nanosheet film has been fabricated from W foil by a simple thermal heating method. The resulting film displays a remarkable combination of unique nanostructure, high conductivity and good hydrophilicity. The K_{0.33}WO₃ nanosheet-modified W foil was thus directly used as electrode, at which a fast direct electrochemistry of GOD was successfully realized. A possible mechanism for the fast electrochemistry was proposed. The electrode also showed excellent sensing performance in terms of high sensitivity, low detection limit, fast response and long-term reliability based on direct electrochemistry of GOD. The unique nanostructure, high electrical conductivity along with its good hydrophilicity, thermal stability and inherent biocompatibility, make the K_{0.33}WO₃ nanosheet a promising material for many technological applications such as biosensors, batteries and biofuel cells. Our work not only provides a highly effective route for the direct growth of nanostructured electrodes, but also sets a good example of broadening the application of tungsten bronzes. In the future, studies are necessary to synthesize the nanosheets with various thicknesses and further explore the relationship between the sheet thickness and the sensing performance.

Experimental Section

Synthesis of the Nanosheet Film

The fabrication of K_{0.33}WO₃ nanosheet film was very simple. Firstly, a piece of cleaned W foil (2×2×0.025 cm³) was sonicated in the KOH solution (0.1 M) for 30 min. After dried, it was heated on a hot-plate under ambient conditions at 600 °C for 24 h, under which a vapor–solid mechanism^[40] governed the nanosheet growth.

Characterization

The product was characterized using powder XRD (Bruker D-8 Avance, Cu_{Kα} radiation; λ=1.5418 Å), TEM (JEM-2010FEF, 200 kV), SEM (JSM-6700F, 5.0 kV), Raman spectroscopy (Witech CRM200, 532 nm), contact-angle meter (FTA 1000), and AFM (Veeco). For TEM tests, the nanosheets were first lightly scraped from the substrate with a blade and mixed with ethanol. Then, a drop of the

sample was placed on a copper mesh coated with an amorphous carbon film, followed by evaporation of the solvent. For I - V test of single nanosheets, a FET device was used; the as-grown $K_{0.33}WO_3$ was removed by sonication from the substrate and subsequently dispersed in ethanol. The solution was dropped on SiO_2/Si (i.e. 200 nm insulated SiO_2 film over Si substrate, gate electrode), and then two Au contact pads 100 nm thick were fabricated by photolithography and rf-sputtering (as source and drain electrodes). The electrical transport property was measured by means of a Suss probe station with Keithley 4200 SCS.

Electrochemical Measurements

For protein immobilization, $K_{0.33}WO_3$ nanosheet film on W electrode was first wetted by 0.01 M phosphate buffer solution (PBS, pH 7.0) and dried by high-purity N_2 gas. 5 μ L GOD (40 units mg^{-1}) solution (15 $mg mL^{-1}$ in 0.01 M PBS, pH 7.0) was then dropped onto the electrode surface. After the evaporation of water, the electrode was stored at 4 °C for one day. The electrochemical properties were examined with a dual-channel electrochemical workstation (CHI 760) using a conventional three-electrode system, which consists of a Pt wire as the counter electrode, a saturated calomel electrode (SCE) as the reference, and a $0.25 \times 0.5 \text{ cm}^2$ $K_{0.33}WO_3$ film on W as the working electrode. Prior to the measurement, a 5 μ L 0.5 w% Nafion solution was further introduced as a backbone to give stable and homogeneously cast thin film. For the direct electrochemistry test, the solution was purged with N_2 for 30 min first to deplete dissolved oxygen. After the purge, a continuous stream of N_2 was introduced into the cell above the liquid surface to maintain an inert atmosphere over the testing solution.

Acknowledgements

This work is financially supported by National Key Basic Research Program of China (973 Program) under contract No.2013CB127804, Institute for Clean Energy & Advanced Materials (Southwest University, Chongqing, China), Chongqing Key Laboratory for Advanced Materials and Technologies of Clean Energies (Chongqing, China), Start-up grant under SWU111071 from Southwest University (Chongqing, China), Chongqing Engineering Research Center for Rapid diagnosis of Dread Disease (Chongqing, China) and Chongqing development and reform commission (Chongqing, China).

Keywords: biosensors · electron transfer · hotplate synthesis · nanostructures · thin films

- [1] I. Willner, B. Willner, *Trends Biotechnol.* **2001**, *19*, 222–230.
- [2] Y. Qiao, C. M. Li, S. J. Bao, Z. S. Lu, Y. H. Hong, *Chem. Commun.* **2008**, 1290–1292.
- [3] Y. Liu, Y. Du, C. M. Li, *Electroanal.* **2013**, *25*, 815–831.
- [4] C. M. Li, C. S. Cha, *Front. Biosci.* **2004**, *9*, 3324–3330.
- [5] J. T. Zhang, C. M. Li, *Chem. Soc. Rev.* **2012**, *41*, 7016–7031.
- [6] X. Q. Cui, C. M. Li, J. F. Zang, S. C. Yu, *Biosens. Bioelectron.* **2007**, *22*, 3288–3292.
- [7] S. J. Bao, C. X. Guo, C. M. Li, *RSC Adv.* **2012**, *2*, 1014–1020.
- [8] J. F. Zang, C. M. Li, X. Q. Cui, J. X. Wang, X. W. Sun, H. Dong, C. Q. Sun, *Electroanalysis* **2007**, *19*, 1008–1014.
- [9] X. J. Zhang, H. X. Ju, J. Wang, *Electrochemical Sensors, Biosensors and Their Biomedical Applications*, Elsevier, New York, **2008**.
- [10] J. J. Gooding, R. Wibowo, J. Q. Liu, W. R. Yang, D. Losic, S. Orbons, F. J. Mearns, J. G. Shapter, D. B. Hibbert, *J. Am. Chem. Soc.* **2003**, *125*, 9006–9007.
- [11] V. Vamvakaki, K. Tsagaraki, N. Chaniotakis, *Anal. Chem.* **2006**, *78*, 5538–5542.
- [12] S. Wu, H. X. Ju, Y. Liu, *Adv. Funct. Mater.* **2007**, *17*, 585–592.
- [13] C. M. Li, W. H. Hu, *J. Electroanal. Chem.* **2013**, *688*, 20–31.
- [14] Y. Liu, M. K. Wang, F. Zhao, Z. A. Xu, S. J. Dong, *Biosens. Bioelectron.* **2005**, *21*, 984–988.
- [15] S. Zhao, K. Zhang, Y. Bai, W. W. Yang, C. Q. Sun, *Bioelectrochemistry* **2006**, *69*, 158–163.
- [16] J. B. Jia, B. Q. Wang, A. G. Wu, G. J. Cheng, Z. Li, S. J. Dong, *Anal. Chem.* **2002**, *74*, 2217–2223.
- [17] W. Y. Cai, L. D. Feng, S. H. Liu, J. J. Zhu, *Adv. Funct. Mater.* **2008**, *18*, 3127–3136.
- [18] S. J. Bao, C. M. Li, J. F. Zang, X. Q. Cui, Y. Qiao, J. Guo, *Adv. Funct. Mater.* **2008**, *18*, 591–599.
- [19] S. Liu, A. Chen, *Langmuir* **2005**, *21*, 8409–8413.
- [20] J. X. Wang, X. W. Sun, A. Wei, Y. Lei, X. P. Cai, C. M. Li, Z. L. Dong, *Appl. Phys. Lett.* **2006**, *88*, 233106–233108.
- [21] A. H. Liu, M. D. Wei, I. Honma, H. S. Zhou, *Anal. Chem.* **2005**, *77*, 8068–8074.
- [22] L. Zhang, Q. Zhang, J. H. Li, *Adv. Funct. Mater.* **2007**, *17*, 1958–1965.
- [23] K. A. Carrado, S. M. Macha, D. M. Tiede, *Chem. Mater.* **2004**, *16*, 2559–2566.
- [24] C. V. Kumar, A. Chaudhari, *J. Am. Chem. Soc.* **2000**, *122*, 830–837.
- [25] J. P. Liu, C. X. Guo, C. M. Li, Y. Y. Li, Q. B. Chi, X. T. Huang, L. Liao, T. Yu, *Electrochem. Commun.* **2009**, *11*, 202–205.
- [26] W. Z. Jia, M. Guo, Z. Zheng, T. Yu, Y. Wang, E. G. Rodriguez, Y. Lei, *Electroanalysis* **2008**, *20*, 2153–2157.
- [27] W. Z. Jia, M. Guo, Z. Zheng, T. Yu, E. G. Rodriguez, Y. Wang, Y. Lei, *J. Electroanal. Chem.* **2009**, *625*, 27–32.
- [28] B. G. Choi, H. Park, T. J. Park, M. H. Yang, J. S. Kim, Y. Jiang, N. S. Heo, S. Y. Lee, J. Kong, W. H. Hong, *ACS Nano* **2010**, *4*, 2910–2918.
- [29] J. C. Claussen, A. D. Franklin, A. ul Haque, D. M. Porterfield, T. S. Fisher, *ACS Nano* **2009**, *3*, 37–44.
- [30] D. B. Luo, L. Z. Wu, J. F. Zhi, *ACS Nano* **2009**, *3*, 2121–2128.
- [31] S. K. Deb, *Appl. Opt. Suppl.* **1969**, *3*, 192–195.
- [32] L. H. Cadwell, R. C. Morris, W. G. Moulton, *Phys. Rev. B* **1981**, *23*, 2219–2223.
- [33] S. Reich, Y. Tsabba, *Eur. Phys. J. B* **1999**, *9*, 1–4.
- [34] T. Kudo, A. Kishimoto, H. Inoue, *Solid State Ionics* **1990**, *40–41*, 567–571.
- [35] L. D. Muhlestein, G. C. Danielson, *Phys. Rev.* **1967**, *158*, 825.
- [36] S. V. Vakarín, A. N. Baraboshkin, K. A. Kaliev, V. G. Zyrianov, *J. Cryst. Growth* **1995**, *151*, 121–126.
- [37] Z. J. Gu, Y. Ma, T. Y. Zhai, B. F. Gao, W. S. Yang, J. N. Yao, *Chem. Eur. J.* **2006**, *12*, 7717–7723.
- [38] H. Qi, C. Y. Wang, J. Liu, *Adv. Mater.* **2003**, *15*, 411–414.
- [39] Z. Zheng, B. Yan, J. X. Zhang, Y. M. You, C. T. Lim, Z. X. Shen, T. Yu, *Adv. Mater.* **2008**, *20*, 352–356.
- [40] T. Yu, Y. W. Zhu, X. J. Xu, K. S. Yeong, Z. X. Shen, P. Chen, C. T. Lim, J. T. L. Thong, C. H. Sow, *Small* **2006**, *2*, 80–84.
- [41] G. Z. Shen, D. Chen, *J. Am. Chem. Soc.* **2006**, *128*, 11762–11763.
- [42] J. Q. Hu, Y. Bando, J. H. Zhan, Y. B. Li, T. Sekiguchi, *Appl. Phys. Lett.* **2003**, *83*, 4414–4416.
- [43] X. S. Fang, C. H. Ye, L. D. Zhang, J. X. Zhang, J. W. Zhao, P. Yan, *Small* **2005**, *1*, 422–428.
- [44] A. Heller, *Acc. Chem. Res.* **1990**, *23*, 128–134.
- [45] S. Wu, J. Wu, Y. Y. Liu, H. X. Ju, *Chem. Mater.* **2008**, *20*, 1397–1403.
- [46] B. Willner, E. Katz, I. Willner, *Curr. Opin. Biotechnol.* **2006**, *17*, 589–596.
- [47] J. Lu, L. T. Drzal, R. M. Worden, I. Lee, *Chem. Mater.* **2007**, *19*, 6240–6246.
- [48] L. Liao, Z. Zhang, Y. Yang, B. Yan, H. T. Cao, L. L. Chen, G. P. Li, T. Wu, Z. X. Shen, B. K. Tay, T. Yu, X. W. Sun, *J. Appl. Phys.* **2008**, *104*, 076104–076106.
- [49] R. Fan, X. H. Chen, Z. Gui, Z. Sun, S. Y. Li, Z. Y. Chen, *J. Phys. Chem. Solids* **2000**, *61*, 2029–2033.
- [50] J. Wang, A. S. Arribas, *Small* **2006**, *2*, 129–134.
- [51] J. Lu, I. Do, L. T. Drzal, R. M. Worden, I. Lee, *ACS Nano* **2008**, *2*, 1825–1832.

- [52] S. Hrapovic, Y. L. Liu, K. B. Male, J. H. T. Luong, *Anal. Chem.* **2004**, *76*, 1083–1088.
- [53] A. Guiseppi-Elie, C. Lei, R. H. Baughman, *Nanotechnology* **2002**, *13*, 559–564.
- [54] J. L. K. Clark, C. Lyons, *Ann. N. Y. Acad. Sci.* **1962**, *102*, 29–45.
- [55] B. Liang, L. Fang, G. Yang, Y. C. Hu, X. S. Guo, X. S. Ye, *Biosens. Bioelectron.* **2013**, *43*, 131–136.
- [56] C. M. Li, H. Dong, X. D. Cao, J. H. Luong, X. Zhang, *Curr. Med. Chem.* **2007**, *14*, 937–951.
- [57] C. X. Guo, C. M. Li, *Phys. Chem. Chem. Phys.* **2010**, *12*, 12153–12159.

Received: April 3, 2013

Published online on July 1, 2013